Neutralization of a negative charge in the S1–S2 region of the $K_V7.2$ (KCNQ2) channel affects voltage-dependent activation in neonatal epilepsy

Thomas V. Wuttke[1,2], Johann Penzien[3], Michael Fauler[4], Guiscard Seebohm[5], Frank Lehmann-Horn[4], Holger Lerche[1,4] and Karin Jurkat-Rott[4]

[1]*Neurological Clinic, University of Ulm, Germany*
[2]*Institute of Anatomy, University of Ulm, Germany*
[3]*Pediatric Hospital, Klinikum Augsburg, Germany*
[4]*Institute of Applied Physiology, University of Ulm, Germany*
[5]*Institute of Physiology I, University of Tübingen, Germany*

The voltage-gated potassium channels $K_V7.2$ and $K_V7.3$ (genes *KCNQ2* and *KCNQ3*) constitute a major component of the M-current controlling the firing rate in many neurons. Mutations within these two channel subunits cause benign familial neonatal convulsions (BFNC). Here we identified a novel BFNC-causing mutation (E119G) in the S1–S2 region of $K_V7.2$. Electrophysiological investigations in *Xenopus* oocytes using two-microelectrode voltage clamping revealed that the steady-state activation curves for E119G alone and its coexpressions with $K_V7.2$ and/or $K_V7.3$ wild-type (WT) channels were significantly shifted in the depolarizing direction compared to $K_V7.2$ or $K_V7.2/K_V7.3$. These shifts reduced the relative current amplitudes for mutant channels particularly in the subthreshold range of an action potential (about 45% reduction at −50 mV for E119G compared to $K_V7.2$, and 33% for E119G/$K_V7.3$ compared to $K_V7.2/K_V7.3$ channels). Activation kinetics were significantly slowed for mutant channels. Our results indicate that small changes in channel gating at subthreshold voltages are sufficient to cause neonatal seizures and demonstrate the importance of the M-current for this voltage range. This was confirmed by a computer model predicting an increased burst duration for the mutation. On a molecular level, these results reveal a critical role in voltage sensing of the negatively charged E119 in S1–S2 of $K_V7.2$, a region that – according to molecular modelling – might interact with a positive charge in the S4 segment.

(Resubmitted 26 August 2007; accepted after revision 13 November 2007; first published online 15 November 2007)
Corresponding author K. Jurkat-Rott: Institute of Applied Physiology, University of Ulm, Albert-Einstein-Allee 11, D-89081 Ulm, Germany. Email: karin.jurkat-rott@uni-ulm.de

The *KCNQ* gene family encodes five voltage-gated K^+ channels, recently classified as KV7.1–$K_V7.5$ (Gutman *et al.* 2005). All K_V7 subunits can assemble into functional homomeric potassium channels (Jentsch, 2000). $K_V7.2$–$K_V7.5$, and probably in particular heteromeric $K_V7.2/K_V7.3$ channels constitute a major component of the M-current, a slowly activating and deactivating K^+ current which can be suppressed by the activation of muscarinic acetylcholine receptors (Brown & Adams, 1980; Wang *et al.* 1998). Since neuronal KV7/M-type K^+ channels activate near the threshold of action potential firing without significant inactivation, they can regulate neuronal excitability by antagonizing repetitive firing of neurons during persistent depolarizing inputs in many neurons of the peripheral and central nervous system (Delmas & Brown, 2005).

Mutations in four of the five *KCNQ* genes lead to inherited diseases of heart muscle, the inner ear or the brain, depending on the different expression patterns of the respective channels (Lehmann-Horn & Jurkat-Rott, 1999; Jentsch, 2000). Mutations in *KCNQ2* or *KCNQ3* cause benign familial neonatal convulsions (BFNC) (Biervert *et al.* 1998; Charlier *et al.* 1998; Singh *et al.* 1998; Jentsch, 2000; Steinlein, 2004; Lerche *et al.* 2005), which is characterized by frequent unprovoked seizures typically beginning within the first days of life and resolving after weeks to months. Patients usually have a normal psychomotor development, but learning disabilities or delayed speech development have been observed in a few individuals (Ronen *et al.* 1993), and recently also unfavourable outcomes with mental retardation have been described (Borgatti *et al.* 2004; Steinlein *et al.* 2007).

DOI: 10.1113/jphysiol.2007.143826

Most of the BFNC mutations were identified in *KCNQ2* (Fig. 1*B*) and a few in *KCNQ3*. They reside predominantly in the pore region or the C-terminus (Lerche *et al.* 2005). Functional analyses of many BFNC-causing mutations have demonstrated a large (generally $> 90\%$) reduction of the maximum K^+ current of homomeric mutant subunits without a dominant-negative effect as the main molecular dysfunction, suggesting a mechanism of haploinsufficiency to be responsible for the phenotype (Biervert *et al.* 1998; Charlier *et al.* 1998; Schroeder *et al.* 1998; Singh *et al.* 1998; Lerche *et al.* 1999, 2005; Steinlein, 2004). However, a few mutations with a dominant-negative effect have been described, two of them causing peripheral nerve hyperexcitability with or without BFNC (Dedek *et al.* 2001; Singh *et al.* 2003; Wuttke *et al.* 2007)

Here, molecular genetic analysis in a BFNC family revealed a novel *KCNQ2* mutation, E119G, which resides in the S1–S2 extracellular loop of the channel, a protein region which has not been associated with mutations so far (Fig. 1*B*). Biophysical analysis provided evidence for an important function of E119 in voltage sensing, similar to negative charges in the S2 segment of *Shaker* K^+ channels (Papazian *et al.* 1995). Furthermore, our results provide a human model pointing to the importance of this ion channel for the regulation of neuronal firing properties at subthreshold voltages.

Methods

Subjects

All patients and their unaffected relatives (or their legal representatives) gave written informed consent to participate in the study. All studies conformed to the standards set by the *Declaration of Helsinki*, and all procedures were approved by the Ethical Committee of the University of Ulm, Germany. All available family members were interviewed in person or by telephone by an experienced paediatrician (JP), and epilepsy histories were documented and corroborated by other family members, except for I-2.

In the three-generation Caucasian family (Fig. 1*A*), individual I-2 (51 years old) was reported to be seizure free on a medication with valproic acid since a generalized tonic-clonic seizure 4 years ago, except for one additional seizure when she reduced the medication. No further details of her epilepsy could be obtained. Individual II-2 (32 years old) presented with epileptic seizures with an onset on postnatal day 2 or 3. The seizure semiology was not well remembered by the patient's parents. Epileptic seizures of individual II-3 (26 years old) were recurring during several weeks with an onset on postnatal day 3 and presented with screaming, followed by generalized stiffness with slight cloni of all extremities, cyanosis and tonic upward movement of the eyes. Episodes were

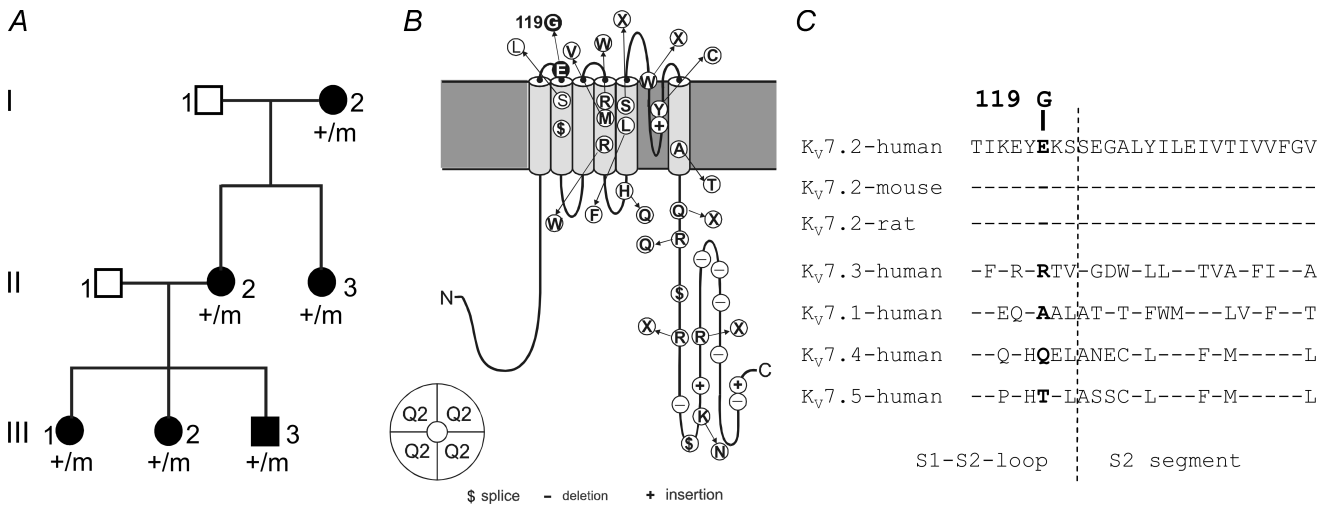

Figure 1. Pedigree, BFNC-causing mutations within the $K_V7.2$ subunit and evolutionary conservation of E119

A, pedigree with clinical and genetic status. +/m: individuals carrying the A→G356 (E119G) mutation. Unaffected individuals are displayed with open symbols, affected ones with filled symbols. *B*, schematic view of a $K_V7.2$ subunit depicting all mutations that have been described so far as white symbols (Borgatti *et al.* 2004; Lerche *et al.* 2005). E119G is marked by a black symbol. *C*, E119 is located within the S1–S2 loop of $K_V7.2$ and is conserved in the orthologous $K_V7.2$ protein of human, mouse and rat. Analogous amino acids are marked in bold. GenBank accession numbers from top are: AY889405, AF490773, AF087453, AF071491, AY114213, AF105216, AF249278.

self-terminating within 2 min. For individual III-1 (9 years old), a first episode with cyanosis and self-limiting cloni involving all four extremities was reported on postnatal day 5. It was followed the next day by three more episodes with generalized cloni which were accentuated on the right-hand side. For individual III-2 (7 years old), seizures started on postnatal day 3 with brief cloni of the right upper extremity and cyanosis of her lips, followed by a second identical episode after 1.5 h. Furthermore, seven generalized motor seizures with cyanosis and cloni were described for postnatal days 4 and 5. Convulsions lasted between 0.5 and 3 min and ceased spontaneously. Patient III-3 (almost 6 years) presented with a brief clonus involving both upper extremities on postnatal day 3 and with episodes of apnoea and cyanosis accompanied by generalized motor seizures on postnatal day 4. All affected individuals, except I-2, were treated with phenobarbital from the day of the first seizure for a period of 1 week up to 3 months. None of them experienced further seizures after discontinuation of the medication, except individual II-3 who experienced several recurrent seizures after discontinuation at the age of 3 months requiring a further 3 months of treatment.

The psychomotor development of all affected individuals was normal. The adults (I-2, II-2, II-3) all finished normal school within regular time. I-2 has been working on the family farm, II-2 was trained as a hair dresser and is now caring for her children, and II-3 is working as a trained saleswoman in a butchery. III-1 and III-2 are going to regular primary school and had good reports. III-3 is entering regular primary school this year.

Mutation analysis

Blood samples were obtained from all six affected family members and DNA was extracted by standard methods. In a candidate gene approach the coding regions and exon–intron boundaries of *KCNQ2* were PCR amplified using previously published PCR primers (Singh *et al.* 2003). Gel-purified products were sequenced on an ABI 3100 automated sequencer. Patient sequences and those of controls were compared to published sequences for *KCNQ2* (GenBank, NM_172107).

Mutagenesis and RNA preparation

Site-directed mutagenesis was used to introduce the amino acid exchange E119G in the *KCNQ* cDNA cloned in the pTLN vector. The insertion of the mutation was verified by automated DNA sequencing. Plasmids were digested with the *Mlu*I restriction enzyme to linearize the DNA. Linearized plasmids were *in vitro* transcribed using the SP6 mMessage mMachine kit (Ambion Inc., Austin, TX, USA) resulting in capped cRNA. Purity was checked by gel electrophoresis. Concentration was verified by spectrophotometry.

Oocyte preparation and injection

All procedures met the National Institutes of Health guidelines for the care and use of laboratory animals and were approved by the Regierungspraesidium Tuebingen, Germany. Female *Xenopus laevis* frogs were anaesthetized with Tricaine (0.1%; Sigma, Deisenhofen, Germany) and placed on ice to maintain anaesthesia. Oocytes were obtained surgically and immediately treated for 2 h with collagenase (2 mg ml^{-1} of type CLS III, Biochrom KG, Berlin, Germany) in OR2-solution (mM: 82.5 NaCl, 2.5 KCl, 1$MgCl_2$ and 5 Hepes, pH 7.6) in order to remove follicular structures. Defolliculated oocytes were stored at 16°C in frog Ringer solution (mM: 115 NaCl, 2.5 KCl, 1.8 $CaCl_2$ and 10 Hepes, pH 7.4) supplemented with 50 μg ml^{-1} gentamycin (Biochrom KG). Diluted cRNA 10–20 ng was injected into each oocyte within 24 h after preparation. Electrophysiological recordings were performed 3 days after injection.

Electrophysiology and data evaluation

Potassium currents were recorded using standard two-microelectrode voltage clamping, a Turbo TEC01C amplifier (npi electronic GmbH, Tamm, Germany) and pCLAMP data acquisition (Axon instruments, Union City, CA, USA), as previously described (Lerche *et al.* 1999). Frog Ringer solution (see above) was used as the bathing solution for all recordings. Recording electrodes were filled with 3 M KCl and had a resistance of 0.3–1 MΩ. Currents were low-pass filtered at 0.3 kHz and sampled at 1 kHz. Oocytes were clamped to a membrane potential of −80 mV followed by depolarizing 10 mV steps up to +20 mV. Tail currents were recorded at −30 mV and their amplitudes analysed to obtain conductance–voltage plots. Data were analysed using pCLAMP 6 with Microsoft Excel, and Origin 6.1 (OriginLab Corp., Northampton, MA, USA) software. A Boltzmann equation was fitted to conductance–voltage relationships: $I/I_{max}(V) = 1/(1 + \exp[(V - V_{0.5})/k])$, with I/I_{max} being the initial normalized tail current amplitude, $V_{0.5}$ the voltage of half-maximal activation and k a slope factor. Time constants of activation and deactivation were obtained by fitting a first order exponential function to the rising phase of the current traces or to the tail current decay. For statistical evaluation two-tailed, unpaired Student's t test was applied ($P < 0.05$ was considered to be significant). All data are shown as means ± S.E.M.

One compartment model for neuronal firing

We implemented a computer model of a one compartment excitable cell according to Golomb *et al.* (2006). The model comprises the following active currents: voltage-gated sodium (I_{Na}) and calcium (I_{Ca}) current, delayed rectifying (I_{DR}), A-type (I_A), M-type (I_M), calcium-dependent (I_C) and afterhyperpolarizing potential (I_{AHP}) potassium current. In contrast to the original model, our I_{Na} also has a slow inactivation gate (Spampanato *et al.* 2004). The M-current is described by a Hodgkin–Huxley type model, with KCNQ/M-channels having one closed and one open state. Then the M-current is given by the following equation:

$$I_M = g_M z^2 (V - V_K),$$

with $g_M = 1\,\mu S\,cm^{-2}$ being the maximal M-current-mediated conductance and $V_K = -91$ mV being the potassium equilibrium potential. V is the membrane potential and z the gating variable of M-channels; z is defined by the following differential equation:

$$\frac{dz}{dt} = \alpha_z (1 - z) - \beta_z z,$$

with

$$\alpha_z = \hat{\alpha}_z \frac{-(V - V\alpha_z)}{1 - e^{-(V - V\alpha_z)/K_{\alpha_z}}} \quad \text{and} \quad \beta_z = \hat{\beta}_z e^{-(V - V_{\beta_z})/K_{\beta_z}}$$

being the forward and backward rates, respectively.

The time constant, τ_z, and the steady-state value, z_∞, are given by:

$$\tau_z = \frac{1}{\alpha_z + \beta_z} \quad \text{and} \quad z_\infty = \frac{\alpha_z}{\alpha_z + \beta_z}.$$

z_∞^2 represents the steady-state activation curve.

To obtain the parameters $\hat{\alpha}_z$, $\hat{\beta}_z$, V_{α_z}, V_{β_z}, K_{α_z} and K_{β_z}, the functions τ_z and z_∞ were simultaneously fitted to the normalized data points, describing (i) the τ_{act}–voltage and τ_{deact}–voltage relationships and (ii) the conductance–voltage relationship, by minimizing the sum of χ^2. We used the data derived from the coexpression experiments of $K_V7.2$ and $K_V7.3$. The results of the fit parameters are given in Table 2. All simulations were realized with Matlab V 7.3 (The MathWorks Inc., Natick, Massachusetts, USA).

Generation of a $K_V7.2$ transmembrane model

The putative position of E119G was estimated using molecular modelling. We generated a homology model of the S1–S6 domains of $K_V7.2$ (*NM_172107*) based on the X-ray coordinates of the $K_V1.2$ K^+ channel crystal structure (PDB ID 2A79; Long *et al.* 2005). At first we generated a model for segments S4–S6 using classical homology modelling based on amino acid similarities between $K_V7.2$ and $K_V1.2$. Since the published structural coordinates of $K_V1.2$ do not provide coordinates of side chains from transmembrane segments S1–S3 and the respective linkers, we generated a peptide chain encoding the amino acids 80–325 of $K_V7.2$ *de novo*. We assigned an α-helical structure to putative transmembrane domains S1–S3. Using the residues glycine and proline as potential kinking points and the positions of the $K_V1.2$ S1–S3 helices as a framework, we were able to position the putative $K_V7.2$ transmembrane segments similarly to the α-helices of the $K_V1.2$ structure. This was achieved by several manual adaptations each followed by energy optimization steps. Force fields used for energy minimizations were GROMOS96 (Deep View/Swiss PDB viewer) and AMBER (BALLVIEW1).

Results

Molecular genetic analysis

Sequence analysis of *KCNQ2* of all affected patients revealed a heterozygous point mutation (A356G) predicting the amino acid substitution of glycine for glutamate at position 119. This mutation was excluded in 96 normal controls by direct sequencing. E119 is located within the S1–S2 extracellular loop of $K_V7.2$ and is evolutionarily conserved in the orthologous mouse and rat $K_V7.2$ channels (Fig. 1*B* and *C*).

Electrophysiology

$K_V7.2$ and $K_V7.3$ WT channels and the E119G mutation were heterologously expressed alone or in various combinations in *Xenopus laevis* oocytes and functionally characterized using a standard two-microelectrode voltage clamp method. Oocytes were depolarized from a holding potential of −80 mV in 10 mV steps up to +20 mV followed by a pulse to −30 mV to record tail currents (Fig. 2*A*). Steady-state activation curves were constructed by analysing tail current amplitudes. The conductance–voltage relationship was significantly shifted towards depolarized voltages for E119G compared to $K_V7.2$ WT channels (Fig. 2*B*), resulting in a reduction of the normalized current amplitudes in the subthreshold range of an action potential between −50 and −30 mV. At −50 mV a highly significant reduction by 45% was observed ($P < 0.0001$, Table 1). The voltage dependence of the kinetics of activation was shifted by approximately +10 mV with a slower activation time course for the mutant channel for potentials between −40 mV and +30 mV (Fig. 2*C*), whereas the deactivation kinetics were not significantly changed (Fig. 2*D*).

To mimic the heterologous condition in a patient carrying one normal and one mutated allele, we also performed coexpressions of E119G with $K_V7.2$ channels.

The depolarizing shifts of both the steady-state activation curve and the kinetics of activation (for potentials between −50 mV and +10 mV) were verified to occur also for the coexpression compared to $K_V7.2$ channels expressed alone, when the same total amount of cRNA was injected in a 1 : 1 ratio (Fig. 2*B* and *C*). Since heteromeric $K_V7.2/K_V7.3$ channels may represent a common correlate of the M-current within the mammalian brain, we additionally evaluated the functional consequences of the E119G mutation for heteromeric conditions with $K_V7.3$ channels. Co-expressions with the same total amount of injected cRNA of E119G with $K_V7.3$ in a 1 : 1, and E119G with $K_V7.2$ and $K_V7.3$ in a 1 : 1 : 2 ratio (to mimic the situation in an affected individual carrying 1 mutant *KCNQ2*, 1 WT *KCNQ2* and 2 WT *KCNQ3* alleles) were compared to a 1 : 1 coexpression of $K_V7.2$ and $K_V7.3$ WT channels. Compared to the data for the homomeric expressions, the results were generally similar but less pronounced. Conductance–voltage curves were still significantly shifted yielding a reduction of the relative current amplitudes at subthreshold voltages for both coexpressions compared to WT channels (Fig. 3*A* and Table 1). At −50 mV, the relative amplitudes were reduced by 33% ($P < 0.01$) and 19% ($P < 0.05$) for E119G/$K_V7.3$ and E119/$K_V7.2/K_V7.3$ compared to $K_V7.2/K_V7.3$ channels, respectively. Also the activation time constants (τ_{act}) were significantly increased (Fig. 3*B*), whereas the deactivation kinetics were not significantly different, although there was a trend towards a slightly faster deactivation for the mutant channel (Fig. 3*C*).

To estimate if there could be additional changes in surface expression induced by the mutation, we

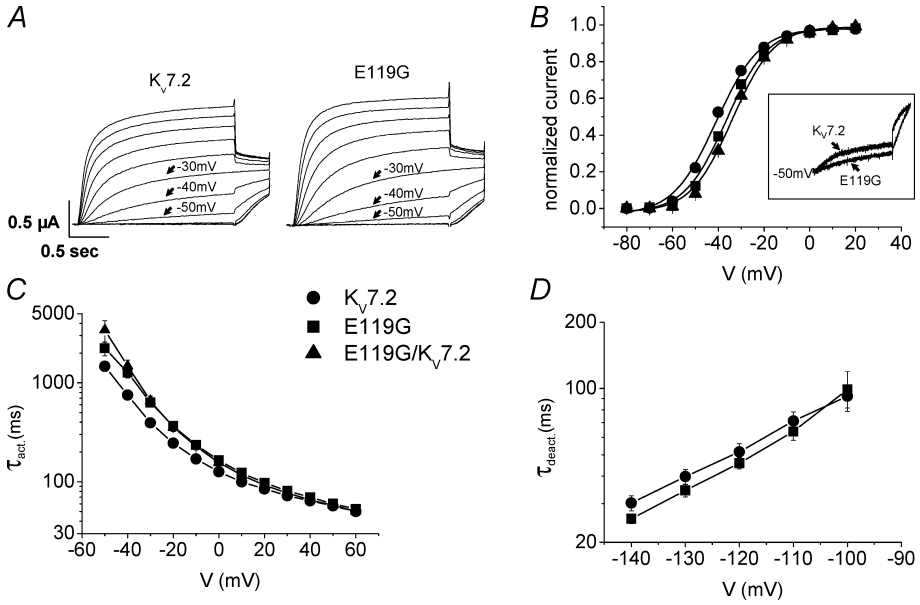

Figure 2. Functional analysis of homomeric and heteromeric $K_V7.2$ WT and mutant channels
A, representative raw current traces for $K_V7.2$ WT and E119G mutated channels. Currents were elicited from a holding potential of −80 mV by depolarizations ranging from −80 to +20 mV in 10 mV steps, followed by a pulse to −30 mV to obtain tail currents. *B*, conductance–voltage curves were constructed by plotting the normalized tail current amplitude recorded at −30 mV against the membrane potential. Lines represent standard Boltzmann functions fitted to the data points. Parameters were as follows: $K_V7.2$ ($n = 12$): $V_{0.5} = -40.7 \pm 0.9$ mV, $k = -8.4 \pm 0.3$ mV; E119G ($n = 18$): $V_{0.5} = -36.4 \pm 0.6$ mV, $k = -8.2 \pm 0.3$ mV; E119G/$K_V7.2$ ($n = 5$): $V_{0.5} = -33.9 \pm 0.8$ mV, $k = -8.1 \pm 0.2$ mV ($P < 0.001$ for $V_{0.5}$ for both conditions with mutant channels *versus* WT). Inset: representative current traces at −50 mV, normalized to the maximal current amplitude at +10 mV, illustrating the difference of current amplitudes. *C*, time constants of activation (τ_{act}) for $K_V7.2$, E119G and the E119G/$K_V7.2$ coexpression were obtained by fitting a first order exponential function to the rising part of each current trace. Values for τ_{act} were plotted against voltage, revealing an about 10 mV rightward shift of the voltage dependence of activation of E119G ($n = 20$) in comparison to $K_V7.2$ ($n = 21$). Activation time constants were significantly different for potentials between −40 mV and 30 mV (−40 mV and 20 mV: $P < 0.01$; −30 mV to 10 mV: $P < 0.001$; 30 mV: $P < 0.05$). For the coexpression of E119G/$K_V7.2$ channels ($n = 5$), the difference from WT $K_V7.2$ channels reached statistical significance for potentials between −50 mV and 10 mV (−50 mV to −30 mV: $P < 0.001$; −20 mV and −10 mV: $P < 0.01$; 0 mV and 10 mV: $P < 0.05$). *D*, time constants of deactivation (τ_{deact}) of $K_V7.2$ ($n = 9$) and E119G ($n = 11$) were evaluated by fitting a first order exponential function to the tail current decay at different potentials after a 1.5 s lasting depolarizing pulse to +50. Values for τ_{deact} were plotted against voltage and did not show a significant difference for potentials ranging between −140 mV and −100 mV. All data are shown as means ± S.E.M.

Table 1. Comparison of normalized current amplitudes in the subthreshold range of an action potential

Channel	Normalized current amplitude		
	−50 mV	−40 mV	−30 mV
$K_V7.2$	0.22 ± 0.02	0.52 ± 0.03	0.75 ± 0.02
E119G	0.12 ± 0.01 (****)	0.39 ± 0.02(***)	0.68 ± 0.02(*)
E119G/$K_V7.2$	0.08 ± 0.01 (***)	0.32 ± 0.02(***)	0.62 ± 0.02(**)
$K_V7.2$/$K_V7.3$	0.21 ± 0.01	0.49 ± 0.02	0.72 ± 0.02
E119G/$K_V7.3$	0.14 ± 0.02 (**)	0.38 ± 0.02(**)	0.64 ± 0.02 (*)
E119G/$K_V7.2$/$K_V7.3$	0.17 ± 0.01 (*)	0.43 ± 0.01(*)	0.68 ± 0.02 (n.s)

Normalized current amplitudes, derived from the activation curves as shown in Figs 2 and 3, of $K_V7.2$ ($n = 12$), E119G ($n = 18$), $K_V7.2$/$K_V7.3$ ($n = 12$) and coexpressions of E119G/$K_V7.2$ (1 : 1 ratio) ($n = 5$), E119G/$K_V7.3$ (1 : 1 ratio) ($n = 8$) or E119G/$K_V7.2$/$K_V7.3$ (1 : 1 : 2 ratio) ($n = 10$) are compared at subthreshold voltages (−50, −40 and −30 mV). A significant reduction of relative current amplitudes was observed for the homomeric E119G channel and for heteromeric channels harbouring the E119G mutant in comparison to $K_V7.2$ or $K_V7.2$/$K_V7.3$ WT channels, respectively. Data are shown as mean ± S.E.M., $^*P < 0.05$; $^{**}P < 0.01$; $^{***}P < 0.001$; $^{****}P < 0.0001$.

evaluated absolute current amplitudes at the end of a 2 s depolarization to 0 mV, a potential at which a plateau in the conductance–voltage relationship was reached (compare Figs 2*B* and 3*A*). Up to three different batches of oocytes were injected with cRNAs coding for WT or mutant channels as monomers or in different combinations. To pool data from different experiments, amplitudes were normalized to the mean one of $K_V7.2$ or $K_V7.2$/$K_V7.3$ that were injected and recorded in parallel with the mutation. Normalized relative amplitudes ranged between 0.7 and 1.8 for $K_V7.2$ and between 0.1 and 1.7 for E119G revealing a broad overlap of data points (Fig. 4). The pooled data from three batches of oocytes revealed a slight but significant decrease for the amplitudes of E119G *versus* $K_V7.2$ ($P < 0.01$). However, this potential mutational effect was not present in any of the coexpression experiments (Fig. 4). In contrast, the depolarizing shift in the voltage dependence of activation and the reduction of relative current amplitudes at subthreshold voltages were consistently found in all of the experiments.

six affected members, thus reflecting a mild phenotype in this family. The disease status completely cosegregated with the mutation indicating a full penetrance. Furthermore, the mutation affected a conserved residue (Fig. 1*B* and *C*) and was not found in a large number of normal controls, so that even without considering the functional data, there is substantial evidence to consider the mutation as disease-causing.

Our electrophysiological investigations showed rather subtle changes of channel gating when compared to other mutations in *KCNQ2* causing BFNC. We found a slight depolarizing shift in steady-state activation and a minor slowing of the activation time course. However, both alterations were consistently found in various coexpression experiments to be statistically significant, so that they have to be considered as real changes due to the mutation. In contrast, there was no evidence for a consistent reduction in maximal current amplitudes, as reported for most of the other BFNC mutations (Biervert *et al.* 1998; Schroeder *et al.* 1998; Lerche *et al.* 1999; Dedek *et al.* 2001; Singh *et al.* 2003; Steinlein, 2004; Lerche *et al.* 2005).

Discussion

Clinical data and pathogenicity of the E119G mutation

Here we identified a novel *KCNQ2* mutation found in a three generation BFNC family with six affected members. The obtainable clinical information on individual I-2 was not sufficient to diagnose BFNC (no history of the neonatal period available), but she had two generalized tonic clonic seizures and carried the mutation so that she can be considered as affected. All other affected individuals presented with an age of onset and seizures typical for BFNC, and psychomotor development was normal in all

Genotype–phenotype correlations in BFNC

As we observed a mild clinical phenotype combined with subtle electrophysiological changes, the question arises whether the increasingly observed unfavourable outcomes with mental retardation (Borgatti *et al.* 2004; Steinlein *et al.* 2007) are associated with a stronger loss of function of M-channels. Borgatti *et al.* (2004) described a mutation with a similar but more pronounced shift of the activation curve, and Steinlein *et al.* (2007) noted

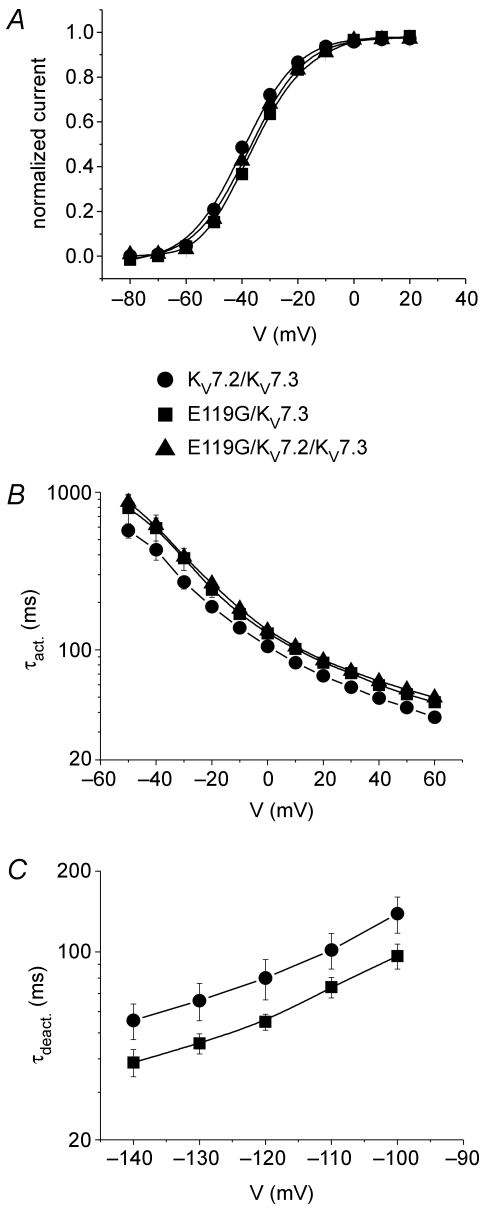

Figure 3. Functional analysis of heteromeric $K_V7.2/K_V7.3$ WT and mutant channels
A, conductance–voltage curves as described in Fig. 2*B* for coexpressions of $K_V7.2/K_V7.3$, E119G/$K_V7.3$ and E119G/$K_V7.2/K_V7.3$ channels. cRNA was injected in either a 1 : 1 or a 1 : 1 : 2 ratio. Lines represent standard Boltzmann functions fitted to the data points. Parameters were as follows: $K_V7.2/K_V7.3$ ($n = 12$): $V_{0.5} = -39.4 \pm 0.7$ mV, $k = -9.3 \pm 0.5$ mV; E119G/$K_V7.3$ ($n = 8$): $V_{0.5} = -35.7 \pm 0.7$ mV ($P < 0.01$), $k = -9.6 \pm 0.9$ mV; E119G/$K_V7.2/K_V7.3$ ($n = 10$): $V_{0.5} = -37.4 \pm 0.5$ mV ($P < 0.05$), $k = -9.1 \pm 0.5$ mV. *B*, time constants of activation (τ_{act}) for $K_V7.2/K_V7.3$ ($n = 12$), E119G/$K_V7.3$ ($n = 9$) and E119G/$K_V7.2/K_V7.3$ ($n = 12$) channels were obtained as described in the legend to Fig. 2. Activation kinetics were slowed for most of the potentials for E119G/$K_V7.3$ (−10 mV to 10 mV: $P < 0.05$; 20 mV to 60 mV: $P < 0.01$) and for E119G/$K_V7.2/K_V7.3$ (−50 mV: $P < 0.05$; −30 mV to 10 mV: $P < 0.01$; 20 mV to 40 mV: $P < 0.001$; 50 mV and 60 mV: $P < 0.0001$) in comparison to $K_V7.2/K_V7.3$ channels. *C*, time constants of deactivation (τ_{deact}) of $K_V7.2/K_V7.3$ ($n = 5$) and E119G/$K_V7.3$ ($n = 6$) were evaluated as described in the legend to Fig. 2 and were not significantly different. All data are shown as means ± S.E.M.

that mutations associated with mental retardation were mainly located in the functionally important S5–S6 region (a functional analysis was not performed in this study). On the other hand, mutations causing a > 90% reduction in $K_V7.2$-mediated current amplitude (when this subunit is expressed alone) are also associated with a good outcome in most cases. Two mutations within the voltage sensor (R207W, R207Q), which induce a very strong slowing and depolarizing shifts of activation with a dominant-negative effect on WT channels, may be the most severe mutations described from an electrophysiological point of view. They are the only mutations causing peripheral nerve hyperexcitability, either with or without BFNC (Dedek *et al.* 2001; Wuttke *et al.* 2007). Two of five individuals (however, genetically identical twins) carrying the most severe R207W mutation have mild learning disabilities (Dedek *et al.* 2001). Thus, mutations with a more severe electrophysiological phenotype might have a tendency to be more often associated with mental retardation, but more solid data with long-term outcomes are necessary to confirm this hypothesis. Other, yet unkown genetic factors could also be responsible for a poor outcome.

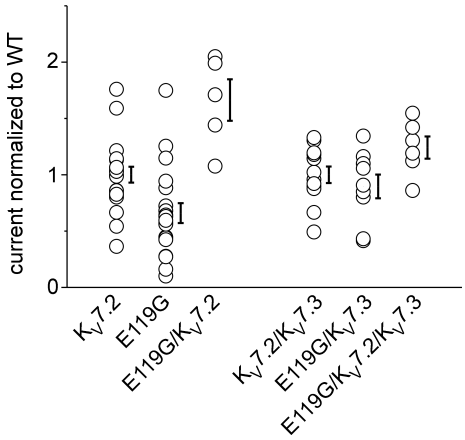

Figure 4. Comparison of maximal current amplitudes
Maximal current amplitudes were analysed after a depolarization lasting 2 s to 0 mV from a holding potential of −80 mV. To pool recordings from different experiments, amplitudes were normalized to the mean value of the amplitudes of $K_V7.2$ or $K_V7.2/K_V7.3$ that were obtained after simultaneous injections and recordings in parallel to the other clones. Co-expressions of the mutation with $K_V7.2$ or $K_V7.3$ were obtained by injection of a constant total amount of RNA in a 1 : 1 or 1 : 1 : 2 ratio in *Xenopus* oocytes. Two to three different batches of oocytes were injected. Normalized amplitudes ranged between 0.4 and 1.8 for $K_V7.2$ ($n = 21$) and between 0.1 and 1.7 for the E119G mutation ($n = 20$) revealing a broad overlap of data points. Pooled data from all batches exhibited a 34% decrease of the mean value of current amplitudes compared to the WT ($P < 0.01$). However, a reduction of the current amplitude could not be confirmed for either heteromeric E119G/$K_V7.2$ ($n = 5$) compared to $K_V7.2$, or E119G/$K_V7.3$ ($n = 9$) and E119G/$K_V7.2/K_V7.3$ ($n = 6$) compared to $K_V7.2/K_V7.3$ channels ($n = 12$). Data are shown as single data points for each oocyte and as means ± S.E.M.

Structure–function considerations suggesting a possible interaction of S1–S2 with S4

These molecular findings suggest the involvement of the S1–S2 region of the $K_V7.2$ channel (probable location of the mutation according to a recent structural model of a mammalian K_V channel (Long *et al.* 2005) and the sequence homologies shown in Fig. 1*C*) in voltage-dependent gating. More specifically, as alterations of the voltage dependence of activation or the time constants of activation are mostly attributed to a modulation of the voltage sensor (Dedek *et al.* 2001; Castaldo *et al.* 2002; Hackos *et al.* 2002; Yellen, 2002; Zhao *et al.* 2004), the question of a possible interaction between S1–S2 and the voltage sensor S4 arises. Negatively charged residues deep within S2 have been shown to interact with positively charged residues of S4 voltage sensors (Papazian *et al.* 1995; Zhang *et al.* 2007), but no such interactions have been proposed thus far for residues located in the adjacent extracellular S1–S2 region. The presence of another BFNC-causing mutation in $K_V7.2$, S122L, which is located just three residues apart from E119 and which shows very similar biophysical changes of voltage-dependent activation to E119G (Hunter *et al.* 2006), may indicate that both S122 and E119 face in the same direction of an α helix and interact with S4.

Table 2. Simulation parameters for the M-current

Symbol	Unit	$K_V7.2/7.3$	E119G/$K_V7.2/K_V7.3$
$\hat{\alpha}_z$	$mV^{-1}\ s^{-1}$	0.239	0.247
$V_{\alpha z}$	mV	−40.6	−25.9
$K_{\alpha z}$	mV	7.8	10.2
$\hat{\beta}_z$	s^{-1}	1.243	1.084
$V_{\beta z}$	mV	−52.4	−49.8
$K_{\beta z}$	mV	31.3	25.5

Results of curve fittings as described in Methods.

To further estimate the position of residues E119 and S122 relative to the S4 segment, we generated a three-dimensional model based on sequence homology for segments S4–S6 and assuming a structural similarity of segments S1–S3 of $K_V7.2$ with the published coordinates of $K_V1.2$ (Fig. 5, Long *et al.* 2005). Whereas the model can be expected to be relatively robust in the S4–S6 region due to the high sequence homology, it is based on a series of assumptions in the S1–S3 region. The assumptions for model generation of S1–S3 are (i) the putative transmembrane domains are α-helices, (ii) the transmembrane domains have a similar position as the transmembrane α-helices in the solved $K_V1.2$ structure, and (iii) the positioning is further determined by the physico-chemical

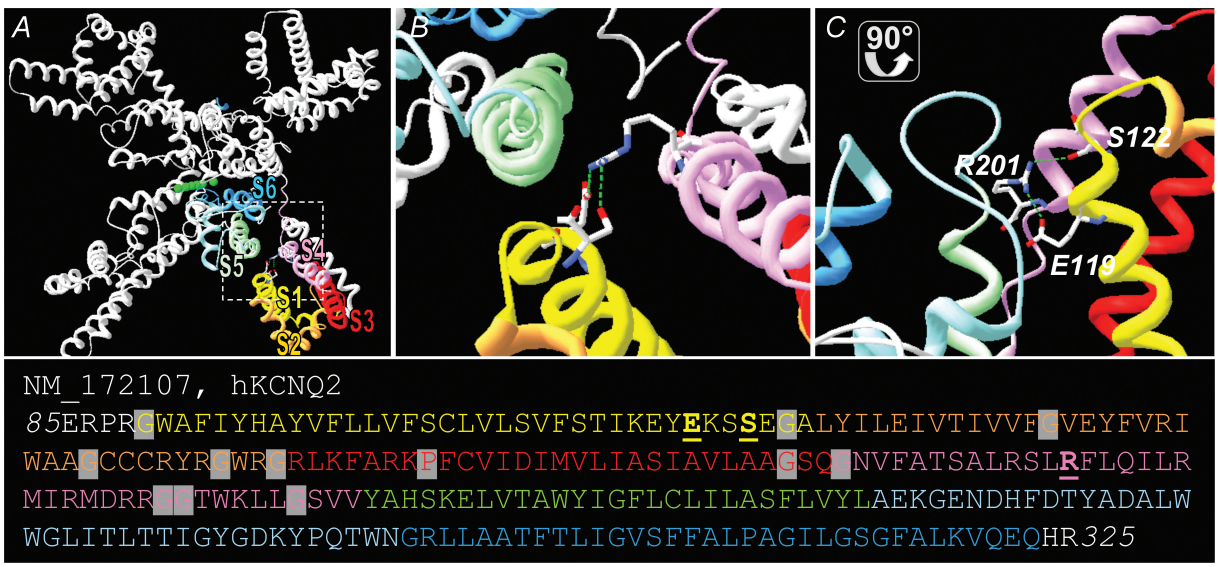

Figure 5. Structural model of the $K_V7.2$ channel
$K_V7.2$ channels were generated based on the coordinates of $K_V1.2$ (PDB ID 2A79; Long *et al.* 2005). The transmembrane segments S1–S4 of one subunit are coloured (S1 (yellow), S2 (orange), S3 (red), S4 (pink) and the pore domain of the adjacent subunit (S5 (green), selectivity filter/pore helix (light blue), S6 (blue)). *A*, overview of 4 subunits. *B* and *C*, magnifications show the putative positions of the residues E119 and S122 in the outer S1 segment and their possible electrostatic interaction or formation of hydrogen bonds with R201 in S4 in top view and side view. Residues E119, S122 and R201 are shown in stick representation (CPK colour code) and putative electrostatic interactions or h-bonds are depicted as green dashed lines. The sequence of $K_V7.2$ is given underneath using the same colours as in the structural model for transmembrane segments. Residues E119, S122 and R201 are printed in bold and underlined. Residues in S1–S4 used to provide flexibility to the model are underlayed in grey.

nature of the linkers and helices (most importantly by the linker length, as defined by the amino acids between two α-helices, and by prolines and glycines providing flexibility and kinks to the structure). These assumptions represent known limitations of the generated model. Based on this model we find the positions of residues E119 and S122 in the outer end of S1 in close proximity to S4 and S5. Particularly, both residues are predicted to be positioned closely to the positively charged arginine R201 of the S4 voltage sensor suggesting either electrostatic interactions or the formation of hydrogen bonds between the respective residues E119/S122 and R201.

These data are consistent with the experimental findings of this and our previous study (Hunter *et al.* 2006) showing that both mutations E119G and S122L induce similar changes in the voltage dependence of activation. However, due to the hypothetical nature of our model such specific interactions remain speculative and have to be interpreted with caution.

Implications of subtle subthreshold changes in M-channel gating

It has been previously suggested that the M-current is involved in the fine regulation of the neuronal membrane potential and that it has a strong impact on spike-frequency adaptation of action potentials at subthreshold voltages, at which not many other channels open (Delmas & Brown, 2005). In this regard, KCNQ/M-channels have been shown to modulate spike afterdepolarization in hippocampal pyramidal neurons (Yue & Yaari, 2004). In contrast to other BFNC-causing mutations which reduce the resulting potassium current over the whole voltage range (Biervert *et al.* 1998; Schroeder *et al.* 1998; Lerche *et al.* 1999, 2005; Dedek *et al.* 2001; Singh *et al.* 2003; Steinlein, 2004), the biophysical changes of E119G and S122L (Hunter *et al.* 2006) are most evident or even restricted to the subthreshold range of an action potential between −60 and −30 mV. Therefore, our data generated from a human disease model strongly support the hypothesis that M-channels act predominantly at subthreshold voltages. The reduction of relative current amplitudes and the slowing of activation lead to a partial loss of function, which can well explain an increase in neuronal firing and the occurrence of epileptic seizures.

To test this hypothesis, we implemented a one compartment cell model to simulate neuronal firing in the presence of M-currents mediated by WT and mutant $K_V7.2$ and $K_V7.3$ channels (see Methods; Spampanato *et al.* 2004; Golomb *et al.* 2006). Under the assumption of an equal expression of WT and mutant channels, we obtained the numeric values of the fit parameters given in Table 2. Figure 6*A* and *B* depicts simulated bursts of action potentials for a constant current injection of 1 μA cm^{-2}. The simulation predicts that M-currents mediated by K_V7 channels act as an early break on repetitive firing and lead to a fast decline of discharge frequency. These effects were less pronounced for the combination of E119G/$K_V7.2$/$K_V7.3$ in comparison to $K_V7.2$/$K_V7.3$ WT channels. Comparing the duration of bursts, elicited by increasing current injection revealed much longer bursts for simulated cells containing mutant channels (Fig. 6*C*). Taken together, these simulations strengthen the hypothesis that even a slight loss of M-current function in the subthreshold range can increase neuronal excitability triggering epileptic seizures in BFNC.

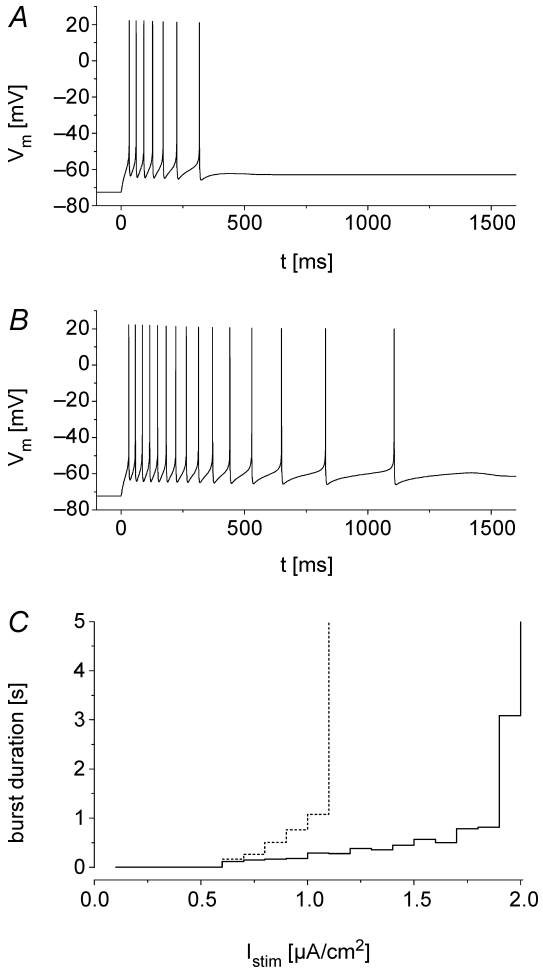

Figure 6. Firing properties in a one compartment neuronal model cell

A and *B*, model cells are continuously stimulated by the current I_{stim} from time $t = 0$ ms. The M-current, I_M, is represented by $K_V7.2$/$K_V7.3$ (*A*) or E119G/$K_V7.2$/$K_V7.3$ (*B*) channels (parameters in Table 2). The duration of the evoked action potential burst is relatively prolonged in cells in which I_M is mediated by E119G/$K_V7.2$/$K_V7.3$ channels. I_{stim} = 1 μA cm^{-2}. *C*, burst duration as a function of I_{stim}. The increase in burst duration with increasing I_{stim} is steeper in cells that are simulated using the mutant channel. There is a threshold above which the M-current is insufficient to terminate the burst. This threshold is lower in simulations with parameters for mutant channels (continuous line $K_V7.2$/$K_V7.3$, dotted line E119G/$K_V7.2$/$K_V7.3$).

References

Biervert C, Schroeder BC, Kubisch C, Berkovic SF, Propping P, Jentsch TJ & Steinlein OK (1998). A potassium channel mutation in neonatal human epilepsy. *Science* **279**, 403–406.

Borgatti R, Zucca C, Cavallini A, Ferrario M, Panzeri C, Castaldo P, Soldovieri MV, Baschirotto C, Bresolin N, Dalla Bernardina B, Taglialatela M & Bassi MT (2004). A novel mutation in KCNQ2 associated with BFNC, drug resistant epilepsy, and mental retardation. *Neurology* **63**, 57–65.

Brown DA & Adams PR (1980). Muscarinic suppression of a novel voltage-sensitive K^+ current in a vertebrate neurone. *Nature* **283**, 673–676.

Castaldo P, Del Giudice EM, Coppola G, Pascotto A, Annunziato L & Taglialatela M (2002). Benign familial neonatal convulsions caused by altered gating of KCNQ2/KCNQ3 potassium channels. *J Neurosci* **22**, RC199.

Charlier C, Singh NA, Ryan SG, Lewis TB, Reus BE, Leach RJ & Leppert M (1998). A pore mutation in a novel KQT-like potassium channel gene in an idiopathic epilepsy family. *Nat Genet* **18**, 53–55.

Dedek K, Kunath B, Kananura C, Reuner U, Jentsch TJ & Steinlein OK (2001). Myokymia and neonatal epilepsy caused by a mutation in the voltage sensor of the KCNQ2 K^+ channel. *Proc Natl Acad Sci U S A* **98**, 12272–12277.

Delmas P & Brown DA (2005). Pathways modulating neural KCNQ/M (Kv7) potassium channels. *Nat Rev Neurosci* **6**, 850–862.

Golomb D, Yue C & Yaari Y (2006). Contribution of persistend Na^+ current to somatic bursting in CA1 pyramidal cells: Combined experimental and modeling study. *J Neurophysiol* **96**, 1912–1926.

Gutman GA, Chandy KG, Grissmer S, Lazdunski M, McKinnon D, Pardo LA, Robertson GA, Rudy B, Sanguinetti MC, Stuhmer W & Wang X (2005). International Union of Pharmacology. LIII. Nomenclature and molecular relationships of voltage-gated potassium channels. *Pharmacol Rev* **57**, 473–508.

Hackos DH, Chang TH & Swartz KJ (2002). Scanning the intracellular S6 activation gate in the shaker K^+ channel. *J Gen Physiol* **119**, 521–532.

Hunter J, Maljevic S, Shankar A, Siegel A, Weissman B, Holt P, Olson L, Lerche H & Escayg A (2006). Subthreshold changes of voltage-dependent activation of the $K_V7.2$ channel in neonatal epilepsy. *Neurobiol Dis* **24**, 194–201.

Jentsch TJ (2000). Neuronal KCNQ potassium channels: physiology and role in disease. *Nat Rev Neurosci* **1**, 21–30.

Lehmann-Horn F & Jurkat-Rott K (1999). Voltage-gated ion channels and hereditary disease. *Physiol Rev* **79**, 1317–1372.

Lerche H, Biervert C, Alekov AK, Schleithoff L, Lindner M, Klinger W, Bretschneider F, Mitrovic N, Jurkat-Rott K, Bode H, Lehmann-Horn F & Steinlein OK (1999). A reduced K^+ current due to a novel mutation in KCNQ2 causes neonatal convulsions. *Ann Neurol* **46**, 305–312.

Lerche H, Weber YG, Jurkat-Rott K & Lehmann-Horn F (2005). Ion channel defects in idiopathic epilepsies. *Curr Pharm Des* **11**, 2737–2752.

Long SB, Campbell EB & Mackinnon R (2005). Crystal structure of a mammalian voltage-dependent Shaker family K^+ channel. *Science* **309**, 897–903.

Papazian DM, Shao XM, Seoh SA, Mock AF, Huang Y & Wainstock DH (1995). Electrostatic interactions of S4 voltage sensor in Shaker K^+ channel. *Neuron* **14**, 1293–1301.

Ronen GM, Rosales TO, Connolly M, Anderson VE & Leppert M (1993). Seizure characteristics in chromosome 20 benign familial neonatal convulsions. *Neurology* **43**, 1355–1360.

Schroeder BC, Kubisch C, Stein V & Jentsch TJ (1998). Moderate loss of function of cyclic-AMP-modulated KCNQ2/KCNQ3 K^+ channels causes epilepsy. *Nature* **396**, 687–690.

Singh NA, Charlier C, Stauffer D, DuPont BR, Leach RJ, Melis R, Ronen GM, Bjerre I, Quattlebaum T, Murphy JV, McHarg ML, Gagnon D, Rosales TO, Peiffer A, Anderson VE & Leppert M (1998). A novel potassium channel gene, KCNQ2, is mutated in an inherited epilepsy of newborns. *Nat Genet* **18**, 25–29.

Singh NA, Westenskow P, Charlier C, Pappas C, Leslie J, Dillon J, Anderson VE, Sanguinetti MC & Leppert MF (2003). KCNQ2 and KCNQ3 potassium channel genes in benign familial neonatal convulsions: expansion of the functional and mutation spectrum. *Brain* **126**, 2726–2737.

Spampanato J, Aradi I, Soltesz I & Goldin AL (2004). Increased neuronal firing in computer simulations of sodium channel mutations that cause generalized epilepsy with febrile seizures plus. *J Neurophysiol* **91**, 2040–2050.

Steinlein OK (2004). Genetic mechanisms that underlie epilepsy. *Nat Rev Neurosci* **5**, 400–408.

Steinlein OK, Conrad C & Weidner B (2007). Benign neonatal convulsions: always benign? *Epilepsy Res* **73**, 245–249.

Wang HS, Pan Z, Shi W, Brown BS, Wymore RS, Cohen IS, Dixon JE & McKinnon D (1998). KCNQ2 and KCNQ3 potassium channel subunits: molecular correlates of the M-channel. *Science* **282**, 1890–1893.

Wuttke TV, Jurkat-Rott K, Paulus W, Garncarek M, Lehmann-Horn F & Lerche H (2007). Peripheral nerve hyperexcitability due to dominant-negative *KCNQ2* mutations. *Neurology* **69**, 2045–2053.

Yellen G (2002). The voltage-gated potassium channels and their relatives. *Nature* **419**, 35–42.

Yue C & Yaari Y (2004). KCNQ/M channels control spike afterdepolarization and burst generation in hippocampal neurons. *J Neurosci* **24**, 4614–4624.

Zhang L, Sato Y, Hessa T, Von Heijne G, Lee JK, Kodama I, Sakaguchi M & Uozumi N (2007). Contribution of hydrophobic and electrostatic interactions to the membrane integration of the Shaker K^+ channel voltage sensor domain. *Proc Natl Acad Sci U S A* **104**, 8263–8268.

Zhao Y, Yarov-Yarovoy V, Scheuer T & Catterall WA (2004). A gating hinge in Na^+ channels; a molecular switch for electrical signaling. *Neuron* **41**, 859–865.

Acknowledgements

We thank all family members who participated in this study and Prof Thomas Jentsch for providing the KCNQ2

and KCNQ3 cDNAs. This study was supported by grants from the Bundesministerium für Bildung und Forschung (BMBF/NGFN2: 01GS0478), the Thyssen-Stiftung, the state Baden-Württemberg (Landesforschungsschwerpunkt 1423/74), the Deutsche Forschungsgemeinschaft (DFG: Le1030/9-1) and the European Union (Epicure: LSH 037315) (to H.L.). T.V.W. was supported in part by a fellowship from the University of Ulm. H.L. is a Heisenberg fellow of the DFG.